JOURNAL OF MATERIALS SCIENCE 25 (1990) 399–406

Effect of mechanical alloying beyond the completion of glass formation for Ni–Zr alloy powders

UICHIRO MIZUTANI, CHUNG HYO LEE
Department of Crystalline Materials of Science, Nagoya University, Furo-cho, Chikusa-ku, Nagoya 464 Japan

Elemental powders of nickel and zirconium were mechanically alloyed over a wide concentration range 10 to 90 at% Zr. The amorphous single phase was formed over the range 20 to 80 at% Zr. The effect of the excessive mechanical alloying on the glass formation was studied by continuing ball-milling beyond the completion of the glass formation for the powders with the average compositions $Ni_{30}Zr_{70}$, $Ni_{50}Zr_{50}$ and $Ni_{70}Zr_{30}$. A partial crystallization took place in all three cases and its initiation was the fastest in $Ni_{30}Zr_{70}$ and was delayed with decreasing zirconium content. The critical factor for triggering the crystallization was attributed to the oxygen contamination for the zirconium-rich $Ni_{30}Zr_{70}$ powders and to the reduction in glass-forming ability for the nickel-rich $Ni_{70}Zr_{30}$ powders. The latter conclusion is drawn from the facts that the impurity concentrations arising from the debris of the stainless steel balls and the vial are gradually accumulated with increasing milling time and that the effective zirconium concentration is reduced below the critical concentration of approximately 20 at% as a result of alloying with the elements iron, chromium and nickel in the stainless steel.

1. Introduction

Mechanical alloying has been recognized as a new technique for synthesizing non-equilibrium materials through solid state diffusion under intense mechanical deformations. Koch *et al.* [1] showed that amorphous alloy powders can be formed by the chemical alloying (MA) of a mixture of elemental powders of nickel and niobium at 60/40 atomic proportion. Since then, the amorphous alloy powders have been produced by MA in a large number of alloy systems, particularly those in which a heat of mixing is negative. This is because the underlying principle for the formation of an amorphous phase by MA is believed to be essentially identical to the now well-established solid state amorphization process in binary diffusion couples [2].

We realise that an amorphous phase can also be formed by ball-milling when the powders of a stable intermetallic compound like $Ni_{50}Zr_{50}$ are employed as starting materials (this may be distinguished from MA and referred to as the mechanical grinding, MG). In contrast to the situation in the MA process, the free energy of the intermetallic compound is the lowest at ambient temperature and, hence, the ball-milling should involve a process which raises the free energy through a yet unknown mechanism upon the formation of an amorphous phase. This addresses the question as to whether or not an amorphous phase obtained by the MA or MG remains stable, if the ball-milling is extended far beyond the completion of the glass formation.

The MA and MG techniques have been applied extensively to the Ni–Zr binary alloy system [3–10]. A comparison of atomic structure [6], thermal and physical [5, 7] properties has been made with the corresponding amorphous alloy prepared by the ordinary liquid quenching (LQ). All these results are essentially consistent with the conclusion that MA (or MG) and LQ result in microscopically almost identical amorphous states.

One of the most serious drawbacks lies in the fact that powdered samples subjected to MA or MG treatment are prone to contamination by various impurities. Brüning *et al.* [9] pointed out that the Ni–Zr powders suffer from oxygen contamination of 2 to 3 at % even when the ball-milling is preformed in a purified argon gas atmosphere and that this causes substantial differences in the crystallization behaviour and also in the superconducting transition temperature. As another source of contamination we should be well aware of impurities due to debris produced during high-energy collisions of the balls themselves and of balls against the wall of the vial. In the present work, we studied the MA and MG processes, using Ni–Zr alloys over a wide composition range. Emphasis is laid on the findings that an amorphous phase produced by MA begins to crystallize as a result of the excessive high-energy ball-milling and that the crystallization involved is deeply related to the introduction of impurities picked up during the MA or MG treatment.

2. Experimental details

Elemental nickel (99.8%, average size 4 to 7 μm) and zirconium (98%, average size 10 μm) powders were mixed at a desired composition and put in a stainless

0022–2461/90 $03.00 + .12

steel vial (18% Cr and 8% Ni) with the inner diameter of 65 mm, together with 20 stainless steel balls with a diameter of 11 mm. The mixed powders were transferred to the vial in a purified argon gas atmosphere. Alloy ingots $Ni_{30}Zr_{70}$ and $Ni_{70}Zr_{30}$ were also prepared by arc-melting in an argon atmosphere. They were broken into pieces and subjected to ball-milling or the MG treatment in the same manner as that for elemental powders.

The vials were mounted on a planetary ball-mill (Fritsch, Pulverisette 5). Its intensity can be controlled by its meter ranging from 0 to 10. The intensity of 9, being equivalent to the vial rotation of 710 r.p.m., was employed, unless otherwise stated. For comparison, the lower intensity of 6 or 500 r.p.m. was also used for the $Ni_{70}Zr_{30}$ powders. The milling was performed at room temperature for 5 h at 2 h intervals and repeated in this cycle. The temperature on the surface of the vial immediately after 5 h ball-milling was checked to be at most 150° C and, hence, was much lower than the crystallization temperatures of 300 to 500° C. Small amounts of the powder samples were taken out in the glove box filled with argon gas during the 2 h intervals for the various analyses described below.

The X-ray diffraction patterns were taken using Cu$K\alpha$ radiation. The morphology of the particles and their chemical compositions were studied using the scanning electron microscope in combination with electron microprobe analysis (EPMA). The crystallization temperature was determined by differential thermal analysis (DTA) with a heating speed of $30° C min^{-1}$.

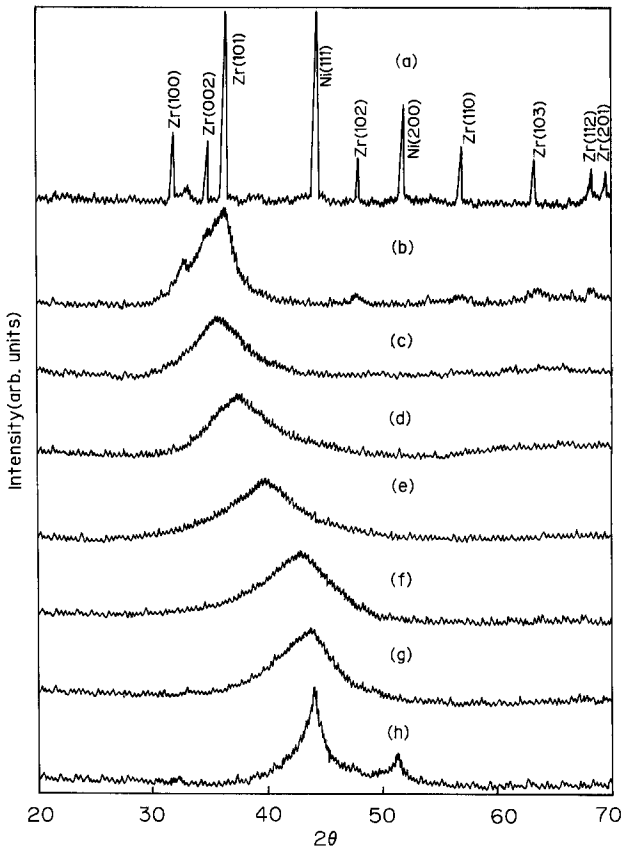

Figure 1 X-ray diffraction patterns for Ni_xZr_{100-x} powders treated by MA with an intensity of 9 for all cases except for $x = 70$ where an intensity of 6 was used. The data shown were obtained after MA treatment for 15 to 20 h. (a) $x = 50$ before MA, (b) $x = 10$, (c) $x = 20$, (d) $x = 30$, (e) $x = 50$, (f) $x = 70$, (g) $x = 80$, (h) $x = 90$.

3. Results and discussion

3.1. Glass formation in Ni–Zr alloy system

Glass formation was attempted using the MA technique for mixtures of nickel and zirconium powders with different average compositions. The results at the completion of the glass formation are illustrated in Fig. 1. The composition range, where an amorphous single phase is formed, was found to extend to 20 to 80 at % Zr in the present experiment. The glass formation is completed in every case after 15 to 20 h ball-milling with an intensity of 9, except for the $Ni_{70}Zr_{30}$ sample for which an intensity of 6 had to be employed to avoid the formation of the intermetallic compound Ni_3Zr. The position of a first peak was found to displace gradually to a higher 2θ value with increasing nickel concentration, reflecting the reduction in an average atomic distance caused by the replacement of a larger zirconium by a smaller nickel atom [5, 11].

The crystallization temperature, T_x, was determined from the exothermic peak observed in DTA measurements and plotted in Fig. 2 as a function of nickel concentration, along with the data of Petzoldt *et al.* [8]. A good agreement is obtained. The value of T_x increases with increasing nickel content up to about 60 at % and then tends to decrease with further increase in nickel content. There is apparently no anomalous minimum near 50 at % Zr in contrast to the data for the liquid-quenched amorphous samples reported by Altounian *et al.* [12], which is indicated by a dashed curve in Fig. 2.

3.2. MA treatment beyond the completion of the glass formation

The effect of excessive milling on the amorphous phase obtained by both MA and MG treatments was, studied using powders with compositions $Ni_{30}Zr_{70}$, $Ni_{50}Zr_{50}$ and $Ni_{70}Zr_{30}$. The products obtained by the MA treatment with an intensity of 9 (modes B and D for $Ni_{30}Zr_{70}$ and $Ni_{70}Zr_{30}$, respectively) are summarized in Fig. 3 for these three alloys as a function of milling time, along with the iron impurity content analysed by EPMA. It clearly shows that the crystallization occurs due to the excessive milling in all three

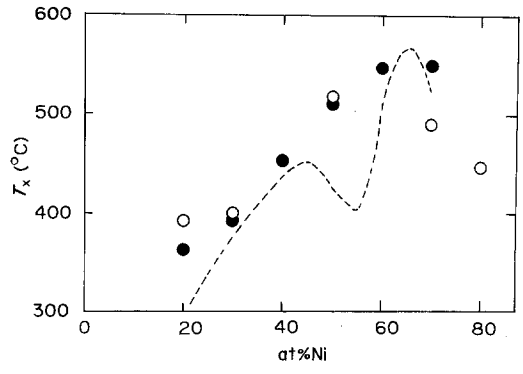

Figure 2 Crystallization temperature, T_x, as a function of nickel content for amorphous Ni_xZr_{100-x} powders produced by MA treatment. The present data (○) are deduced from the DTA measurement with a heating speed of $30° C min^{-1}$. (●) Data for MA amorphous powders obtained by Petzoldt *et al.* [8]. (– – –) Data for LQ amorphous alloys obtained by Altounian *et al.* [12].

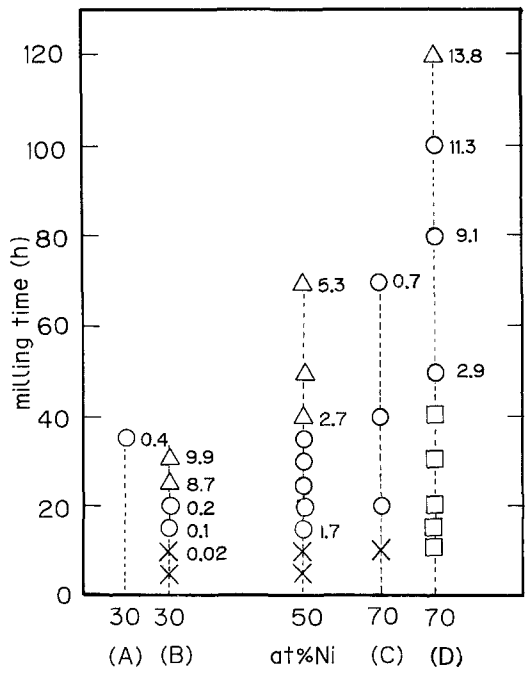

Figure 3 Phases of mechanically alloyed Ni_xZr_{100-x} powders as a function of accumulated milling time. An intensity of 9 was employed, unless otherwise stated. (x) pure elemental nickel and/or zirconium remains, (○) amorphous single phase, (△) partially crystallized powders, and (□) powders containing $NiZr_3$ intermetallic compound. Modes (A) and (B) refer to the MA processes without and with opening of the vial in a glove box every 5 h, respectively. Modes (C) and (D) refer to the ball-milling with intensities of 6 and 9, respectively.

cases, although the milling time required is the shortest in the $Ni_{30}Zr_{70}$ and increases with decreasing zirconium content. It can also be seen that the iron content increases with increasing total milling time. Although not indicated in Fig. 3, the chromium impurity is also detected and its content is always about one-fourth that of the iron impurity. We will discuss more details below for the respective alloys.

3.2.1. $Ni_{30}Zr_{70}$

Fig. 4 shows the X-ray diffraction data for the $Ni_{30}Zr_{70}$ powders as a function of accumulated milling time. An amorphous phase once formed begins to crystallize when the milling is continued beyond the completion of the glass formation or the total milling time exceeds 25 to 30 h.

The change in the morphology of MA particles was studied as a function of milling time. Fig. 5 shows the scanning electron micrographs for the $Ni_{30}Zr_{70}$ powders treated by MA 15 and 30 h. As recognized from Fig. 4, the former corresponds to an amorphous single phase whereas the latter involves the partial crystallization. The particle in an amorphous state is fairly round and its size distribution is centred at about 50 μm diameter. In contrast, the partially crystallized particle is more irregular and sharper and its size distribution is much broader.

The chemical composition and impurities were checked by EMPA. In both amorphous and partially

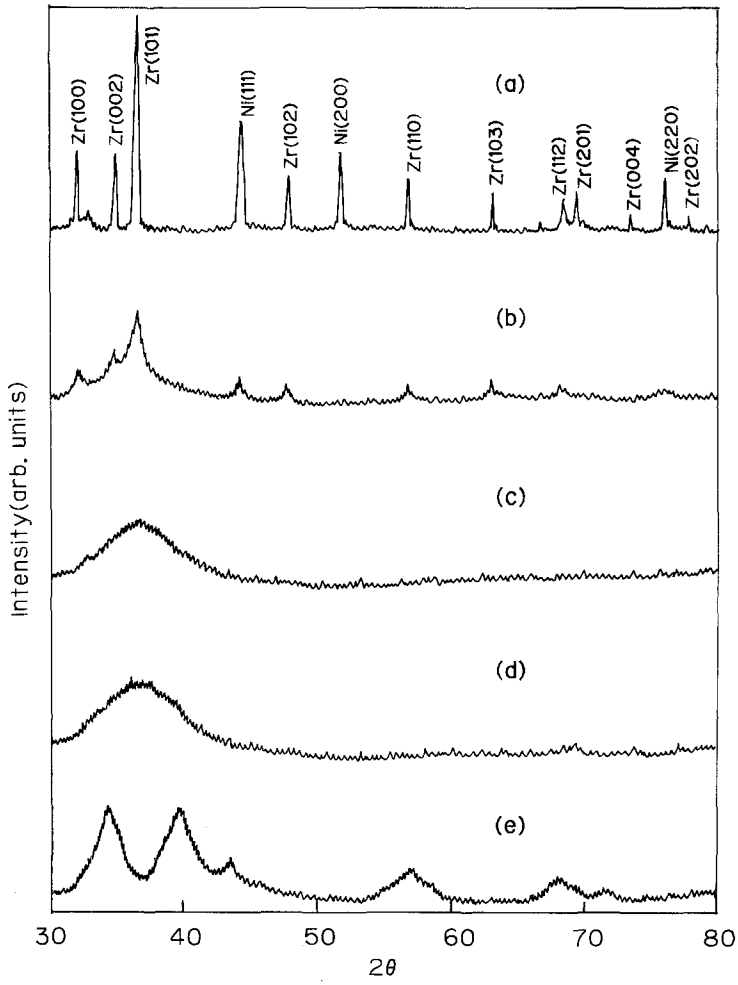

Figure 4 X-ray diffraction patterns for MA powders $Ni_{30}Zr_{70}$ as a function of total milling time. Mode (B) in Fig. 3 was used. (a) $t = 0$, (b) $t = 10$ h, (c) $t = 15$ h, (d) $t = 20$ h, (e) $t = 30$ h.

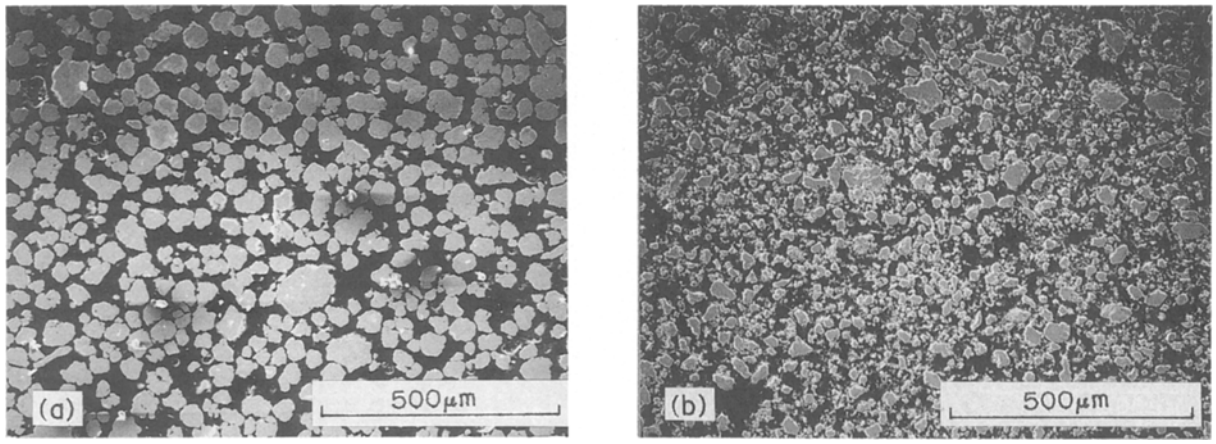

Figure 5 Scanning electron micrographs for $Ni_{30}Zr_{70}$ powders treated by MA for (a) 15 h and (b) 30 h. Mode (B) in Fig. 3 was used.

crystallized particles, the composition fluctuations of two constituent elements nickel and zirconium were not detected within a particle, indicating that they distribute uniformly in an amorphous matrix and that the partial crystallization does not result in a large scale segregation beyond the resolution of a few micrometres in EPMA. As is clear from Fig. 3, the amount of iron impurities increases enormously after crystallization and reaches 8 to 9 at %, the level being almost 100 times as high as that (0.1 at %) in the amorphous state. Furthermore, smaller particles seen in the scanning electron micrograph for partially crystallized powders are found to contain more iron than the average, whereas larger ones contain the same level as in the amorphous powders.

The $Ni_{30}Zr_{70}$ elemental powders were also ball-milled totally for 35 h in the same conditions as described above but without opening the vial in the glove box at all. Here the powders were kept all the time under a purified argon gas atmosphere in the vial during the MA treatment. As shown in Fig. 3 (mode A), the resulting powders were found to remain amorphous without any indication of crystallization. Furthermore, the level of the iron impurity was kept suppressed below 0.4 at %. This indicates that neither heating during the MA treatment nor milling time is a crucial factor for crystallization.

We consider that the opening of the vial in the glove box every 5 h to pick up samples for X-ray analysis introduces some oxygen and moisture, which most likely cover a fresh surface of MA powders. When the milling is continued beyond the glass formation, powders start to stick to the wall of the vial and no longer stay as free particles at the bottom of the vial. The milling is thus carried out as if no powders were in the vial. The crystallization apparently takes place, when this occurs. Once crystallization proceeds, the sample on the wall begins to fall off again and forms irregular particles. Therefore, we believe that the amorphous phase produced by the MA treatment remains stable, even though the milling time with the high intensity, is extended but that partial crystallization is more likely to be induced when oxygen is introduced into the system and the powders begin to stick to the wall. This change in the milling conditions apparently accelerates the diffusion of oxygen and also the introduction of iron and chromium impurities arising from the stainless steel balls and the wall of the vial.

3.2.2. $Ni_{50}Zr_{50}$

According to Fig. 3, the $Ni_{50}Zr_{50}$ elemental powders become amorphous after 15 h. Although the vial was opened every 5 h in the glove box, the powders did not stick to the wall of the vial and an amorphous single phase was maintained until the total milling time exceeded 40 h. After that, the powders began to stick on the wall and crystallization commenced. Hence, the reaction is essentially the same as that observed in the $Ni_{30}Zr_{70}$ discussed above, except that the critical time for the onset of crystallization is delayed to 40 h. The iron content increased again here in harmony with the crystallization.

3.2.3. $Ni_{70}Zr_{30}$

The situation in the $Ni_{70}Zr_{30}$ is entirely different. As shown in Fig. 6, the X-ray diffraction lines for 10 h MA powders can be identified as the Ni_3Zr intermetallic compound, indicating that the solid state diffusion leads first to the formation of a stable crystalline phase exisiting in the phase diagram. An important note here is that the intermetallic compound Ni_3Zr is formed only when the high intensity of 9 is employed, but without involving oxygen contami-nation, because it was formed even when the ball-milling was performed for 10 h without opening the vial in the glove box during the interval. It was also realised that the powders almost completely stuck to the wall in the first 10 h and that the small amount of powder formed in the bottom of the vial turned out to be the intermetallic compound mentioned above. Further MA treatment exceeding a total milling time of 20 h resulted in almost free particles. The X-ray diffraction data for 50 h MA powders indicate that the powders become almost completely amorphous and that the amorphous phase remained stable until the milling time reached 100 h. However, crystallization did occur even in this nickel-rich sample, when the total milling time exceeded 120 h (see mode D in Fig. 3). As shown in Fig. 3, the iron content for the $Ni_{70}Zr_{30}$ powders increases gradually as a function of milling time, even when the powders maintain an amorphous phase.

Schultz [7] recently reported similar observations

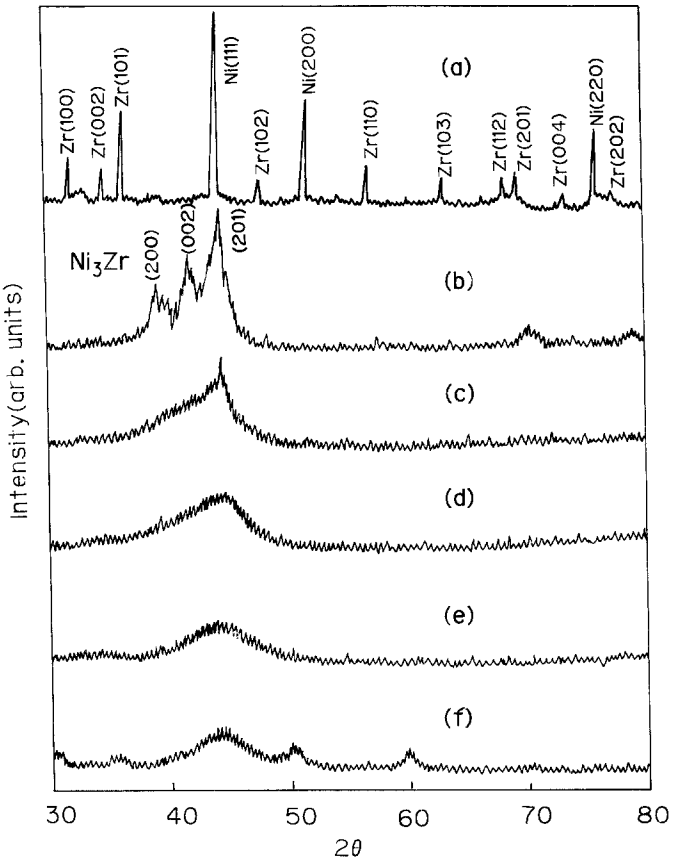

Figure 6 X-ray diffraction patterns for MA powders $Ni_{70}Zr_{30}$ as a function of total milling time. Mode (D) in Fig. 3 was used. (a) t = 0, (b) t = 10 h, (c) t = 30 h, (d) t = 50 h, (e) t = 100 h, (f) t = 120 h.

in the Ni_xZr_{100-x} alloy system. Using the same ball-milling machine as we employed, he found that the elemental powders in the range x = 65 to 75 became partially crystallized when its intensity was increased to 7 or 570 r.p.m. From this he suggested that the excessive heating is likely to be responsible for the crystallization. The X-ray diffraction pattern for the $Ni_{70}Zr_{30}$ powders after the 10 h MA treatment is essentially identical to that observed by Schultz. We revealed in this experiment that further MA treatment led to glass formation. This clearly indicates that the excessive heating should not be the cause of crystallization. We must also note that an amorphous single phase can be formed after 20 h MA treatment without involving the intermetallic compound when the intensity is reduced to 6, the results of which have already been discussed in connection with the data shown in Fig. 1. The mechanism for the unique dependence of the MA product on the ball-milling intensity is not clear at this stage.

3.3. Thermal studies of the crystallized phase caused by excessive milling

3.3.1. $Ni_{30}Zr_{70}$

The partially crystallized powders obtained after 30 h MA treatment were heat-treated in vacuum at various temperatures for 10 to 40 h, in order to facilitate identification of the crystallized phase caused by excessive milling. The results are shown in Fig. 7. First of all, it is of interest to note that the diffraction peaks in the partially crystallized powders (Fig. 7a) reduce their intensities with increasing annealing temperature up to 500° C but new peaks start to grow above about 430° C (Fig. 7c). When the powders are annealed at 600° C, the diffraction lines become fairly sharp. The diffraction lines for powders annealed at 800° C (Fig. 7f) were carefully analysed in comparison with the data for amorphous powders produced by 15 h MA treatment and subsequently subjected to the same

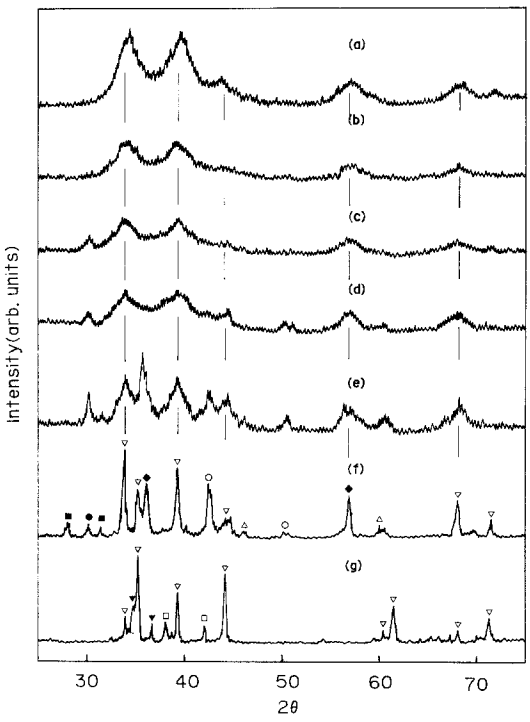

Figure 7 X-ray diffraction patterns for MA powders $Ni_{30}Zr_{70}$ subjected to various heat-treatments. (a) Partially crystallized powders after 30 h MA treatment (see Fig. 4e); (b) to (f) powders of (a) annealed in vacuum at (b) 400° C, 20 h, (c) 430° C, 40 h, (d) 500° C, 20 h, (e) 600° C, 20 h, (f) 800° C, 10 h; and (g) an amorphous single-phase powder (Fig. 4c) annealed in vacuum at 800° C for 10 h. (▽) $NiZr_2$, (□) α-Zr, (△) ω-Zr, (◆) hexagonal Zr_3O, (●) tetragonal ZrO_2, (■) monoclinic ZrO_2, (▼) $Ni_{22}Zr_{67}O_{11}$, and (○) a phase containing a large amount of iron and chromium impurities.

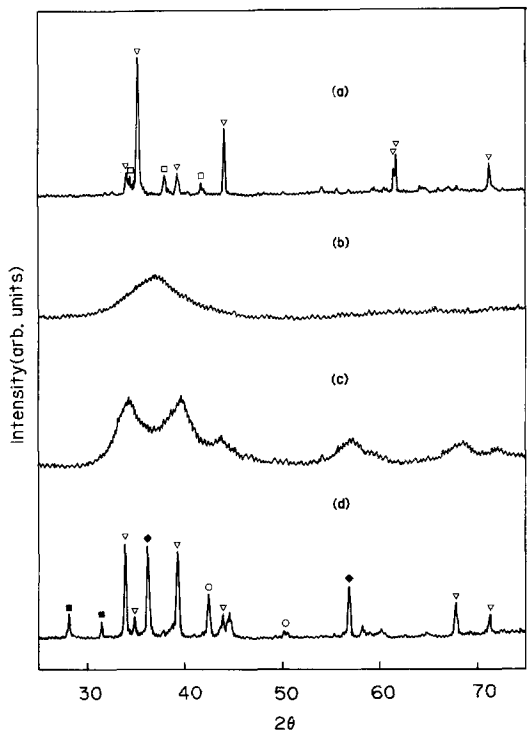

Figure 8 X-ray diffraction patterns for MG powders $Ni_{30}Zr_{70}$. (a) Alloy ingot annealed at 800° C for 10 h in vacuum, (b) powders subjected to MG for 15 h, (c) powders subjected to MG for 34 h and (d) powders of (c) annealed in vacuum at 800° C for 10 h. (▽) $NiZr_2$, (■) monoclinic ZrO_2, (◆) hexagonal Zr_3O, (□) α-Zr, and (○) a phase containing large amounts of iron and chromium impurities.

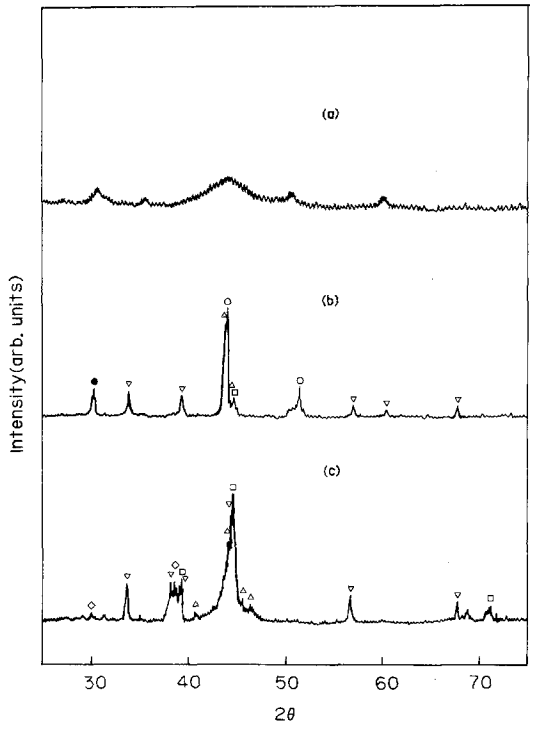

Figure 9 X-ray diffraction patterns for MA powders $Ni_{70}Zr_{30}$. (a) Powders obtained by 120 h MA treatment, (b) powders of (a) subjected to annealing in vacuum at 800° C for 10 h, and (c) amorphous powders obtained by 40 h MA treatment with mode (C) in Fig. 3 with subsequent annealing in vacuum at 900° C for 10 h. (▽) $Ni_{10}Zr_7$, (△) $Ni_{21}Zr_8$, (□) Ni_3Zr, (◇) Ni_7Zr_2, (●) tetragonal ZrO_2, and (○) a phase containing large amounts of iron and chromium impurities.

annealing conditions (Fig. 7g). The latter can be indexed in terms of the tetragonal $NiZr_2$ and α-Zr, which are naturally understood from the phase diagram as products resulting from the phase separation at 800° C. A trace of the γ-phase oxide $Ni_{22}Zr_{67}O_{11}$ [13] also seems to be present.

In contrast, the diffraction lines for the partially crystallized powders after 800° C heat treatment are no longer identical. All diffraction lines associated with α-Zr apparently disappear and, instead, the lines of zirconium-oxides, i.e. tetragonal and monoclinic ZrO_2 and hexagonal Zr_3O are formed. Nevertheless, the $NiZr_2$ compound definitely coexists with these zirconium oxides. By tracing back the change in the diffraction profile as a function of annealing temperature, we are naturally led to conclude that the crystallized phase caused by the excessive milling is most likely identified as the compound $NiZr_2$. In addition, it may be worthwhile mentioning that the lines at $2\theta = 43°$ and 51° cannot be uniquely identified but most likely represent a phase containing substantial iron and chromium impurities.

Keeping the above findings in mind, we attempted to perform the X-ray diffraction analysis for powders produced by the MG treatment, using the alloy ingot as starting materials. As shown in Fig. 8, diffraction lines before the MG treatment are essentially identical to those of Fig. 7g. In other words, the as-prepared ingot contains only α-Zr and $NiZr_2$ without any zirconium oxides. We revealed that an amorphous single phase can easily be formed after 15 h MG treatment. However, partial crystallization did occur when the MG treatment exceeded 30 h (note that the vial was opened every 5 h in the glove box). As is seen from Fig. 8d, the annealing of the partially crystallized powders at 800° C for 10 h led to the same diffraction pattern as that of Fig. 7f. From all these experiments we conclude that the oxygen contamination in the zirconium-rich Ni–Zr powders is quite serious and leads to the crystallization of an amorphous phase once formed.

3.3.2. $Ni_{70}Zr_{30}$

As shown in Fig. 6, the partial crystallization commenced when the MA treatment exceeded 120 h. The powders thus obtained were annealed at 800° C for 10 h. The diffraction lines for the annealed powders are shown in Fig. 9b. They can be indexed in terms of $Ni_{10}Zr_7$ [14], $Ni_{21}Zr_8$ [15] and Ni_3Zr [16] plus some additional lines, which cannot be positively identified. As mentioned earlier, we consider that the lines at $2\theta = 44°$ and 51° are most likely associated with the phase containing iron and chromium impurities arising from the stainless steel. Note that, as shown in Fig. 3, the EMPA analysis revealed the average iron content of 13.7 at % and chromium content of 3.6 at %, indicating that iron and chromium are substantially contained in this sample.

Fig. 9c refers to the diffraction lines for the amorphous powders heat-treated at 900° C for 10 h in vacuum. Here, we employed amorphous powders obtained by 40 h MA in mode C (see Fig. 3), which contain less than 1 at % iron and chromium impurities. The diffraction lines centred near $2\theta = 38°$ and 44° are not well resolved, even though the annealing

temperature is chosen 100° C higher than that in Fig. 9b. The equilibrium compounds $Ni_{10}Zr_7$ and $Ni_{21}Zr_8$ are apparently present. They are naturally understood as the decomposition of the amorphous powders with the average composition of 30 at % Zr [16]. It is of interest to note that Ni_3Zr and Ni_7Zr_2 also appear, even though these two compounds are located outside the two-phase field. This might be taken as an indication that nickel-rich regions are locally present in the amorphous matrix.

We direct our attention to the difference in the diffraction lines between (b) and (c) in Fig. 9. The peak at $2\theta = 51°$ associated with the phase containing iron and chromium is absent in (c). It is recalled that this peak appears only in the crystallized powders containing sustantial iron and chromium impurities (see also Fig. 7). In the $Ni_{70}Zr_{30}$ powders, the amorphous single phase is maintained over a much longer milling time than in the $Ni_{30}Zr_{70}$, during which they accumulate a substantial amount of iron and chromium impurities. The debris from the stainless steel should contain not only iron and chromium but also nickel atoms. Hence, we consider that the total content of three elements iron, chromium and nickel in the 120 h MA powders most likely exceeds 80 at %. As will be discussed in the next section, we believe that these impurities dissolve in the sample and cause the zirconium content to reduce below 20 at %. Here it may be recalled from Fig. 1 that the glass-forming ability is substantially reduced, when the zirconium content becomes less than 20 at %. We conclude, therefore, that, in the case of $Ni_{70}Zr_{30}$, the oxygen contamination is less important and that the accumulation of iron and chromium impurities arising from the stainless steel plays a crucial role in triggering the crystallization due to excessive milling.

3.4. Iron and chromium impurities in amorphous phase

It is now quite evident that the intense ball milling introduces iron and chromium impurities to the powder sample. The amount of these impurities cannot be negligible even in the amorphous phase, particularly, for the $Ni_{70}Zr_{30}$ powders subjected to the ball-milling with an intensity of 9 (see mode D in Fig. 3). Nevertheless, the X-ray diffraction shows only a halo pattern without any indication of crystalline phases associated with the stainless steel. This suggests that these impurities are dissolved in the amorphous matrix at the atomic level.

To gain further insight into the nature of iron and chromium impurities in the amorphous matrix, we analysed the X-ray diffraction data by employing the hard sphere approximation. The atomic radii of nickel, iron, chromium and zirconium are 0.125, 0.128, 0.129 and 0.160 nm, respectively [17]. Thus, the atomic sizes of the three elements nickel, iron and chromium are hardly distinguishable but are much smaller than that of zirconium. If the iron and chromium impurities are dissolved at the atomic level, then the zirconium concentration should be reduced and its reduction would be reflected in the position of the first peak in the X-ray diffraction pattern or the corresponding

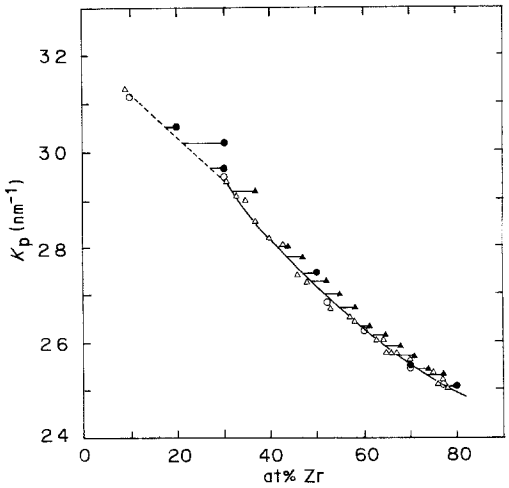

Figure 10 The K_p value as a function of zirconium concentration for LQ amorphous ribbons measured by Buschow (△) and in our laboratory (○). Included are the present data for MA amorphous powders (●) and the data obtained by Weeber and Bakker [5] (▲). A smooth curve and a dashed line are drawn through the data points for LQ amorphous alloys. A horizontal short line refers to the concentration shift caused by the introduction of iron, chromium and nickel impurities.

wavenumber, K_p. We employed the K_p value derived for the liquid-quenched amorphous ribbons [11, 18] as a reference and compared it with the data for the MA powders, because the former is free from such impurities.

Fig. 10 shows the K_p values as a function of zirconium concentration for LQ amorphous alloys, together with those for amorphous alloys prepared by the MA treatment in the present experiment and also those reported by Webber and Bakker [5]. It is seen that the data for the LQ amorphous alloys fall on a universal curve in the zirconium concentration range from 30 to 80 at %. Data for the range 10 to 30 at % Zr are missing because of the difficulty in making an amorphous single-phase alloy by liquid quenching. However, the value of K_p at 10 at % Zr is known and the value obtained by Buschow [11] agrees well with ours [18]. Hence, we connected the K_p values at 10 and 30 at % Zr by a straight line and have used it as part of the reference curve.

The zirconium concentration in Fig. 10 for the MA amorphous powders refers to the nominal one, without taking into account the iron and chromium impurities. As a result, the K_p value is found to deviate consistently to the right from the reference curve. This is true not only for the present samples but also for those reported by Weeber and Bakker [5]. A short horizontal line shown in Fig. 10 represents the concentration difference, Δx, and can be taken as a measure for the reduction in zirconium concentration as a result of the introduction of iron, chromium and nickel atoms from the stainless steel (Webber and Bakker employed a steel ball and vial and, hence, only iron impurity has to be considered in their data).

Fig. 11 shows the value of Δx against the total impurity concentration of iron and chromium revealed by EPMA for the present amorphous powders and also for those by Weeber and Bakker. The fact that the data roughly fall on a line passing through the

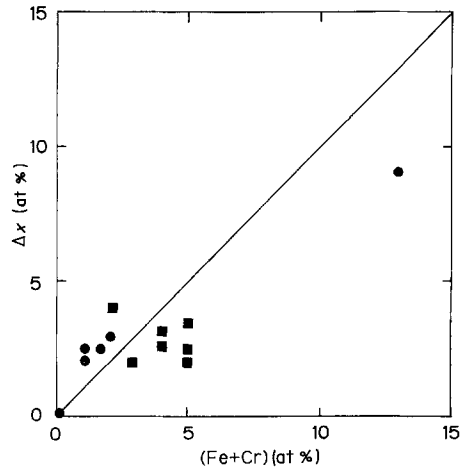

Figure 11 Zirconium concentration shift, Δx, as a function of total iron and chromium content revealed by EPMA for the present MA amorphous powders (●) and for those obtained by Weeber and Bakker [5] (■).

origin supports the validity of the present analysis and strengthens our argument that the iron and chromium impurities are completely alloyed in the amorphous matrix.

4. Conclusion

We have revealed that the Ni–Zr amorphous powders produced by the MA or MG treatment begin to crystallize when the ball-milling is continued beyond the completion of the glass formation. Oxygen contamination is responsible for the crystallization in the zirconium-rich $Ni_{30}Zr_{70}$ amorphous powders, whereas the accumulation of iron and chromium impurities beyond the critical concentration pushes the zirconium concentration out of the glass-forming range and leads to crystallization for the nickel-rich $Ni_{70}Zr_{30}$ amorphous powders.

Acknowledgements

The use of SEM and EPMA facilities was made possible through the courtesy of Dr S.Tanemura, Government Industrial Research Institute, Nagoya, and we are most grateful for this help. The authors also thank Dr T. Nishio and M. Mori, Nagoya University, for their help in the preparation of MA powders and in taking SEM micrographs and EPMA analysis.

References

1. C. C. KOCH, O. B. CAVIN, C. G. McKAMEY and J. O. SCARBROUGH, *Appl. Phys. Lett.* **43** (1983) 1017.
2. R. B. SCHWARZ and W. L. JOHNSON, *Phys. Rev. Lett.* **51** (1983) 415.
3. A. W. WEEBER, H. BAKKER and F. R. DE BOER, *Europhys.* **2** (1986) 445.
4. A. W. WEEBER, H. BAKKER, H. J. M. HEIJLIGERS and G. F. BASTIN, *Europhys. Lett.* **3** (1987) 1261.
5. A. W. WEEBER and H. BAKKER, *J. Phys.* **F18** (1988) 1359.
6. F. ITOH, T. SEKIUCHI, M. SAKURAI, T. FUKUNAGA and K. SUZUKI, Proceedings of the 5th Japan Institute of Metals International Symposium on Non-Equilibrium Solid Phases of Metals and Alloys, Kyoto, March, 1988. Supplement to Trans. JIM, Vol. 29 (1988) 127.
7. L. SCHULTZ, *Mater. Sci. Engng* **97** (1988) 15.
8. F. PETZOLDT, B. SCHOLZ and H-D. KUNZE, *ibid.* **97** (1988) 25.
9. R. BRÜNING, Z. ALTOUNIAN, J. O. STROMOLSON and L. SCHULTZ, *ibid.* **97** (1988) 317.
10. P. Y. LEE and C. C. KOCH, *J. Mater. Sci.* **23** (1988) 2837.
11. K. H. J. BUSCHOW, *J. Phys.* **F14** (1984) 593.
12. Z. ALTOUNIAN, TU GUO-HUA and J. O. STROMOLSEN, *J. Appl. Phys.* **54** (1983) 3111.
13. M. V. NEVITT and J. W. DOWNEY, *Trans. Met. Soc. AIME* **221** (1961) 1014.
14. M. KIRKPATRICK, J. F. SMITH and W. L. LARSEN, *Acta Crystallogr.* **15** (1962) 894.
15. L. BSENKO, *J. Less-Common Met.* **63** (1979) 171.
16. T. B. MASSALSKI, "Binary Alloy Phase Diagrams", Vol. 2 (American Society for Metals, 1986) p. 1777.
17. The International Union of Crystallography, "International Table for X-ray Crystallography" (Kynock Press, Birmingham, 1962).
18. S. KANEMAKI, O. TAKEHIRA, H. KOMATSU, K. FUKAMICHI and U. MIZUTANI, to be published.

Received 17 October 1988
and accepted 23 January 1989